Removal of an anionic reactive dye from aqueous solution using functionalized multi-walled carbon nanotubes: isotherm and kinetic studies

Shahab Karimifard, Mohammad Reza Alavi Moghaddam*

Civil and Environmental Engineering Department, Amirkabir University of Technology (AUT), Hafez St. Tehran 15875-4413, Iran, emails: Shahab.karimifard@gmail.com (S. Karimifard), alavi@aut.ac.ir, alavim@yahoo.com (M.R. Alavi Moghaddam)

ABSTRACT

In this research, the adsorption process of Reactive Blue 19 (RB19) as an anionic dye onto functionalized multi-walled carbon nanotubes (f-MWCNTs) was studied. For this purpose, four parameters including agitation time, adsorbent dose, initial dye concentration, and pH were examined. N_2 adsorption isotherms and Fourier transform infrared spectroscopy were used to characterize f-MWCNTs. Four isotherm and four kinetic models including two diffusion models were applied to comprehensively investigate the RB19 adsorption using f-MWCNTs. It was found that the adsorption follows Langmuir and Temkin equilibrium models with a maximum adsorption capacity of 217.39 mg g^{-1}. The adsorption process best fitted to pseudo-second-order kinetic model and by applying diffusion models, the predominant rate-limiting step was found to be physisorption during the liquid film diffusion.

Keywords: Adsorption; Anionic dye; Multi-walled carbon nanotubes; Isotherm; Kinetics; Diffusion models

1. Introduction

Reactive dyes are one of the most widely used classes of dyes, especially in the textile industry, which are capable of directly reacting with the fiber substrate and forming strong covalent bonds [1,2]. Because of their high stability, widespread usage, and the large degree of aromatics present in these molecules, effluents containing reactive dyes must be treated appropriately [3]. In aqueous solutions, those reactive dyes which carry a net negative charge due to the presence of sulfonate (SO_3^-) groups, are classified as anionic reactive dyes [4]. Reactive Blue 19 is an anionic reactive dye which is very resistant to decolorization due to the fact that its aromatic anthraquinone structure is highly stabilized by resonance [5]. Also, researchers are concerned about toxicity and mutagenicity of RB19 because of the vinyl sulfone groups present in the RB19 structure [6–10].

Several methods, such as advanced oxidation [7], flocculation [11], photocatalysis [12], electrocoagulation [13], sonolysis [14], and biological processes [15] have been studied for the removal of RB19 from wastewater. Adsorption process is considered to be one of the most effective methods to treat dye-containing wastewater [16–21]. Low cost, simplicity, and high efficiency have made the adsorption process preferable among the other conventional methods for the removal of reactive dyes along with other pollutants from aqueous solutions [22–25]. Some adsorbents like activated carbon [5,26], bentonite [27], chitosan [28],

*Corresponding author.

and wheat bran [29] were used to remove RB19 from aqueous solutions.

Multi-walled carbon nanotubes (MWCNTs) have demonstrated their value as novel and strong adsorbents because of their small size, large specific surface area, negatively charged surface, and hollow/layered structure [30]. MWCNTs are more effective in cationic dye removal because of the attractions between their surface and positively charged dye molecules [31]. On the contrary, the electrostatic interactions between anionic dyes and MWCNTs usually result in low adsorption capacity, inconsistency of outcomes, and inefficiency of the process. To overcome such problem of MWCNTs, different modification methods, such as surfactant treatment [32], magnetizing [33,34], and functionalization [35–37] can be utilized.

To the best of our knowledge, utilizing functionalized MWCNTs (f-MWCNTs) for removal of RB19 has not been studied yet. Therefore, in this study, four isotherm and four kinetic equations including two diffusion models were applied to comprehensively investigate the adsorption process of RB19 onto f-MWCNTs.

2. Materials and methods

2.1. Preparation and characterization of f-MWCNTs

Raw MWCNTs fabricated by CVD method were purchased from Neutrino Corporation, Iran. 0.1 g of pristine MWCNTs was put onto a quartz plate and irradiated in a modified domestic microwave (Samsung, ME201-Malaysia) with power of 100 W for 10 min under a constant airflow of 1,000 mL min^{-1} and was cooled afterward to room temperature. Most of MWCNT surface oxidation activity occurs within the first hour of sonication in acid [38]. Therefore, the irradiated MWCNTs were mixed in 100 mL of 3 M H_2SO_4 and sonicated for 1 h in an ultrasonic bath (Sonoswiss, 90 W, 50–60 Hz-Switzerland). Finally, the slurry was vacuum-filtered through 0.2 μm PTFE filters (Sartorius-Germany) and washed several times with distilled water until no change in pH was observed. The MWCNTs were dried at room temperature (25°C).

The textural properties of f-MWCNTs were investigated by N2 adsorption/desorption isotherms (BET & BJH analysis) at 77 K using a Quantachrome Autosorb 1 analyzer (USA). It was found that the BET specific surface area and BJH pore volume of f-MWCNTs are 343.63 and 0.368 cm^3 g^{-1}, respectively. The Fourier transform infrared spectroscopy (FT-IR) analysis was conducted with a Thermo Nicolet, Nexus 670 (USA) in the spectral range from 4,000 to 600 cm^{-1} on KBr discs
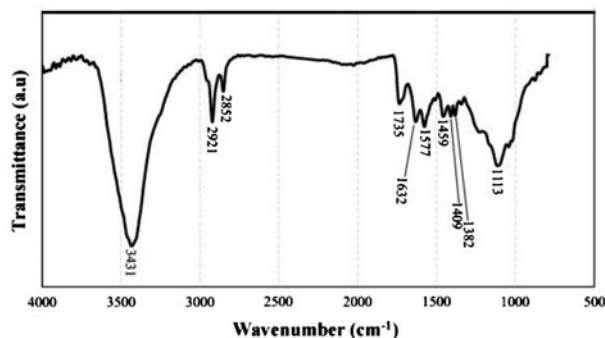

Fig. 1. FT-IR spectra of f-MWCNTs.

and is presented in Fig. 1. The IR spectrum shows important absorption bands at 3,431 cm^{-1} (attributed to OH stretching), 2,921 cm^{-1} (assigned to asymmetric CH_2 stretching), 2,921 and 2,852 cm^{-1} (assigned to C–H alkane stretching), 1,735 cm^{-1} (attributed to C=O stretching), 1,632 cm^{-1} (corresponding to conjugated C=C stretching), 1,577 (corresponding to C=C alkene stretching), 1,459 and 1,382 cm^{-1} (assigned to CH_3 bending), 1,409 cm^{-1} (corresponding to C–H alkene stretching), and 1,113 cm^{-1} (attributed to C–O stretch in alcohols). The introduction of CH_3 groups could be mainly attributed to sonication that cuts and defects the MWCNT's walls, which leads to release of carbons at the defected sites and end points.

2.2. Adsorption procedure of RB19

RB19 was purchased from Alvan Sabet Company, Iran. The properties and chemical structure of RB19 are presented in Table 1. The solution pH was measured using a 340i/SET pH meter (WTW-Germany) and adjusted with H_2SO_4 and NaOH (Merck-Germany). The effect of different pH values (2–12) on RB19 stability

Table 1
The general properties and chemical structure of RB19

Parameters	Values
Molecular formula	$C_{22}H_{16}N_2Na_2O_{11}S_3$
λ_{max} (nm)	594
Molecular weight (MW)	626.54
Chemical structure	
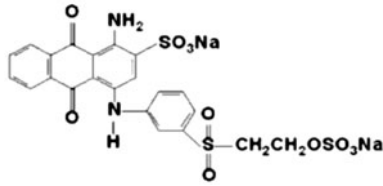
was investigated and it was observed that this dye was stable in this range.

For adsorption batch experiments, 150 mL of RB19 solution and the desired dosage of f-MWCNTs were placed in 250 mL flasks. The solution was sonicated for 5 min to disperse f-MWCNTs, then it was agitated at 150 rpm on a conventional shaker (Edmund Buhler, Germany). Prior to the analysis, the sample was centrifuged at 6,000 rpm for 10 min (Hettich, EBA 21-Germany). RB19 concentration was measured using a HACH spectrophotometer DR/4000 (USA) at a wavelength corresponding to the maximum absorbance of 592 nm ($\lambda_{\max}$). The adsorption studies were carried out at 25 ± 1°C.

2.3. Adsorption isotherm and kinetic models

In this study, four isotherm models including Langmuir, Freundlich, Temkin, and Halsey equations were applied to describe the equilibrium data. In addition, the chi-square error analysis method was applied to all isotherm data. This statistic test is the sum of squares of the differences between the experimental and calculated data, with each squared difference divided by the corresponding data obtained from calculation from models [39]. The mathematical equation of chi-square analysis is:

$$\chi^2 = \sum_{i=1}^{m} \frac{\left(q_{e,\exp} - q_{e,calc}\right)^2}{q_{e,calc}} \tag{1}$$

where $q_{e,\exp}$ is the adsorption capacity at equilibrium (mg g^{-1}), $q_{e,calc}$ is the adsorption capacity obtained from the model's calculation (mg g^{-1}). If the data from the model are similar or close to experimental values, X^2 will be a relatively small number ($0 < X^2 < 5$) [40]. Moreover, four kinetic models including pseudo-first-order, pseudo-second-order, intraparticle diffusion, and liquid film diffusion equations, were used to describe the adsorption rate and determine the rate-controlling step.

3. Results and discussion

3.1. Adsorption of RB19 on f-MWCNTs

The effect of agitation time on the adsorption process of RB19 using f-MWCNTs is illustrated in Fig. 2. This step was accomplished under the following conditions: Adsorbent dose of 0.3 g L^{-1}, initial dye concentration of 50 mg L^{-1}, and pH of 3. The adsorption rate initially increased rapidly and then became approximately constant, as the agitation time elapsed.

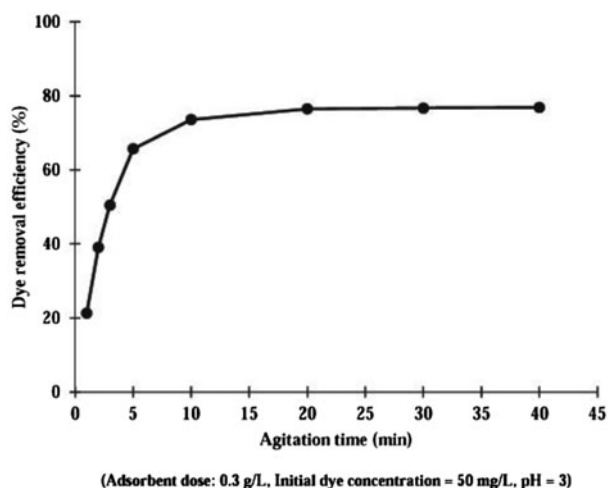(Adsorbent dose: 0.3 g/L, Initial dye concentration = 50 mg/L, pH = 3)

Fig. 2. The effect of agitation time on RB19 removal using f-MWCNTs.

Rapid adsorption in first few minutes is due to the availability of active sites on adsorbent which results in intense electrostatic adsorption of the dye, but with the gradual occupancy of these sites, the adsorption procedure became less efficient [41]. After 20 min, no significant change in adsorption of RB19 was observed; therefore the time of 20 min was adopted for all subsequent experiments.

As presented in Fig. 3, the effect of three selected parameters including adsorbent dose, initial dye concentration, and pH on RB19 adsorption using f-MWCNTs was investigated at a constant agitation time of 20 min. The dye removal efficiency increased with an increase in f-MWCNT dosage (Fig. 3(a)). Increasing adsorbent dosage augments the number of adsorption sites available for adsorption [42]. The dye removal efficiency declined by increasing the initial dye concentration (Fig. 3(b)). At higher concentrations, the number of dye molecules ratio to the available adsorption sites is high and therefore, dye removal efficiency decreases [30]. The maximum dye removal efficiency was achieved at the lowest pH values (Fig. 3(c)). In acidic conditions, enhancement of adsorption efficiency can be due to increasing positively charged sites, which favors the adsorption of anions via electrostatic attractions [43]. Similar results were obtained for removal of RB19 using other adsorbents, such as activated carbon [26], bentonite [27], chitosan [28], and ash of pulp and paper sludge [39].

3.2. Adsorption isotherms

Generally, the adsorption isotherms indicate how the adsorbate molecules are distributed between the
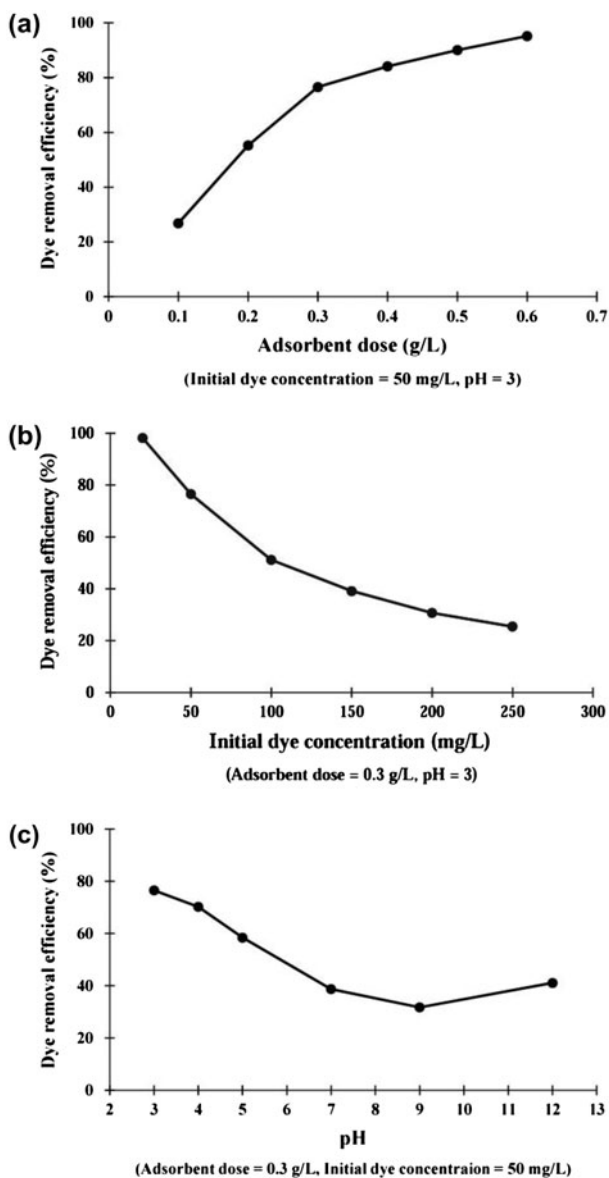
Fig. 3. Effects of (a) adsorbent dose, (b) initial dye concentration, and (c) pH on RB19 removal using f-MWCNTs.

liquid and solid phases when the adsorption procedure reaches an equilibrium state [39]. The isotherm data are analyzed by fitting them into different equilibrium models, which is a significant step for designing purposes [44]. The fitting of experimental data to four isotherm models including Langmuir, Freundlich, Temkin, and Halsey is depicted in Fig. 4. Furthermore, the isotherm formulas and important parameters for RB19 removal using f-MWCNTs are presented in Table 2. More details about each isotherm model are discussed in the following subsections.

3.3. Langmuir isotherm

Langmuir equation mainly relates the coverage of molecules on a solid surface to the concentration of a medium above the solid surface at a constant temperature [42]. This isotherm is based on three general assumptions, namely adsorption process is limited to monolayer coverage, all surface sites are alike which can only accommodate one adsorbed atom, and the adsorption of a molecule on a given site is independent of its neighboring sites' occupancy [45]. The essential features of Langmuir model can be expressed in terms of a dimensionless constant called separation factor (R_L) which is presented as the following equation:

$$R_L = \frac{1}{1 + K_L C_0} \tag{6}$$

where K_L is the Langmuir constant and C_0 (mg L^{-1}) is the highest RB19 concentration. The value of R_L indicates the type of the isotherm to be either unfavorable ($R_L > 1$), Linear ($R_L = 1$), favorable ($0 < R_L < 1$), or irreversible ($R_L = 0$) [45]. As presented in Table 2, a high R^2 value of 0.9971, R_L value of 0.0313 and a very small amount of X^2 demonstrate that Langmuir isotherm describes the adsorption of RB19 on f-MWCNTs almost perfectly.

3.4. Freundlich isotherm

Freundlich equation is an empirical model which refers to the non-ideal and reversible adsorption with non-uniform distribution of adsorption heat and affinities over the heterogeneous surface [46]. A favorable adsorption tends to have n values between 1 and 10 [45]; and a constant outside this range implies an irreversible or unfavorable adsorption [47]. As it is shown in Table 2, the n value of 4.2992 indicates that RB19 is favorably adsorbed by f-MWCNTs.

3.5. Temkin isotherm

Temkin equation is based on two general assumptions, namely the decline of the sorption heat as a function of temperature is linear rather than logarithmic, and the adsorption process is characterized by a uniform distribution of binding energies up to a maximum binding energy [47]. Although the Temkin isotherm is superior in the prediction of gas equilibria [45], several studies used it for dye removal systems in aqueous solutions [39,42,43,47]. Table 2 data imply that the Temkin model with a high R^2 value of 0.9967
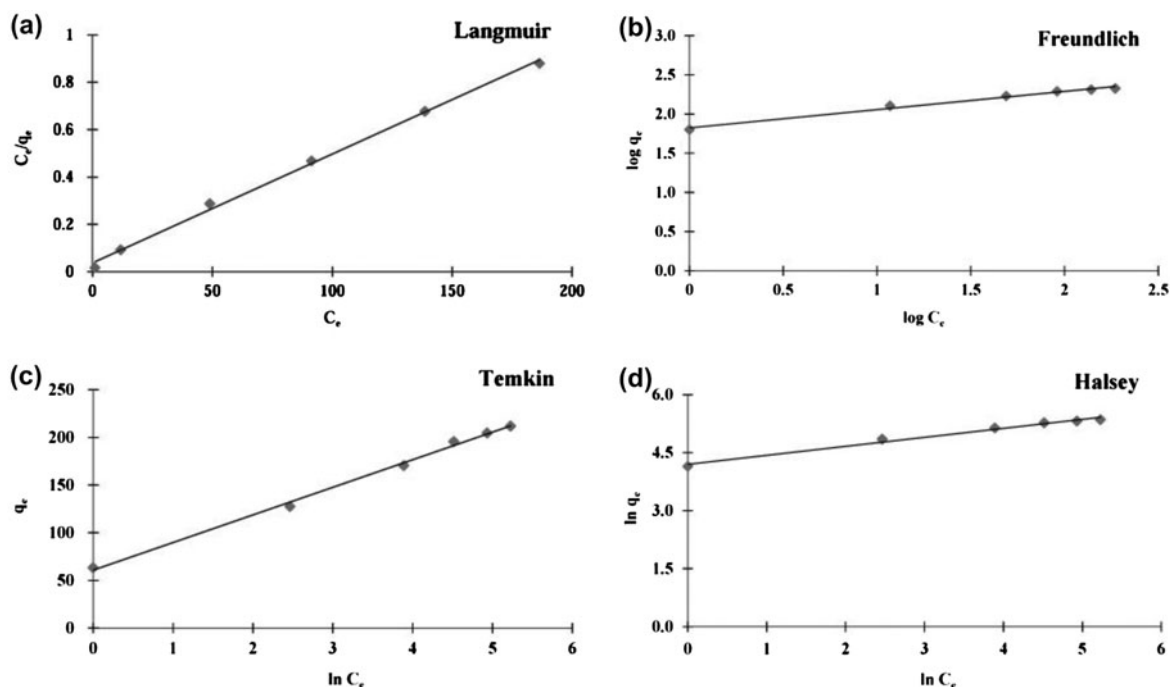
Fig. 4. Isotherm models for RB19 adsorption on f-MWCNTs: (a) Langmuir, (b) Freundlich, (c) Temkin, and (d) Halsey models.

and a very small value of X^2 (0.4084) fits the adsorption procedure very well.

3.6. Halsey isotherm

Halsey proposed an equation for condensation of a multilayer at a relatively large distance from the surface [45]. The Halsey adsorption isotherm is suitable for multilayer adsorption and fitting the experimental data to this equation attests to the heterogeneous nature of the adsorbent [48]. The data in Table 2 suggest that Halsey isotherm is also capable of modeling the adsorption of RB19 onto f-MWCNTs but not preferable among other isotherms.

To conclude, it could be derived from Fig. 4 and Table 2 that Langmuir and Temkin isotherms are the best models to describe the adsorption of RB19 using f-MWCNTs due to their highest R^2 and reasonable X^2 values. This may indicate that the dye removal process is predominantly homogenous and monolayered. In this research, according to Langmuir model, the maximum adsorption capacity of f-MWCNTs was found to be 217.39 mg g^{-1}. This result is relatively high compared to other studies which utilized other adsorbents to remove RB19, such as coconut shell based activated carbon with maximum RB19 uptake of 2.91 mg g^{-1} [5], ash of pulp and paper sludge with an adsorption capacity of 85.81 mg g^{-1} [39], and modified bentonite with a q_{max} of 206.58 mg g^{-1} [27].

3.7. Adsorption kinetics

A kinetic study for adsorption is very important because it provides information regarding efficiency and the possibility of expansion of the process [44]. Moreover, the kinetic parameters are helpful for the prediction of adsorption rate [43]. Thus, in this study, four kinetic equations including two diffusion models were applied to investigate the kinetics of RB19 adsorption onto f-MWCNTs. Their corresponding graphs and parameters are presented in Fig. 5 and Table 3, respectively. More details about each kinetic model are given in the following subsections.

3.8. Pseudo-first-order model

In 1898, Lagergren introduced his kinetic equation which is called pseudo-first-order model. Nowadays, it is the most widely used kinetic model for adsorption of different pollutants [49]. A linear plot of log $(q_e - q_t)$ vs. t is used to determine the rate constants as presented in Fig. 5(a). Table 3 values show that although this model has an acceptable R^2 value, a considerable deviation of experimental and calculated

Table 2
Isotherm models for the adsorption of RB19 onto f-MWCNTs

| Isotherm model	Equation	Definition of equation factors	Important parameters	Values
Langmuir	$\dfrac{C_e}{q_e} = \dfrac{1}{q_{max}} C_e + \dfrac{1}{K_L q_{max}}$　(2)	C_e = Dye concentration at equilibrium (mg L^{-1})	q_{max} K_L R_L R^2 X^2	217.39 0.1239 0.0313 0.9971 1.5875
		q_e = Adsorption capacity at equilibrium (mg g^{-1}) K_L = Langmuir adsorption constant (L mg^{-1}) q_{max} = Calculated maximum adsorption capacity (mg g^{-1})		
Freundlich	$\log q_e = \log K_F + \dfrac{1}{n} \log C_e$　(3)	K_F = Freundlich constant (mg g^{-1})	K_F n R^2 X^2	66.635 4.2992 0.9866 2.1011
Temkin	$q_e = B_1 \ln K_T + B_1 \ln C_e$　(4)	n = The adsorption intensity B_1 = The heat of adsorption dimensionless parameter	K_T B_1 R^2 X^2	8.1580 28.945 0.9967 0.4084
Halsey	$\ln q_e = \dfrac{1}{n_H} \ln K_H - \dfrac{1}{n_H} \ln C_e$　(5)	K_T = The equilibrium binding constant (L mg^{-1}) K_H = Halsey constant (mg L^{-1}) n_H = Halsey equation exponent	K_H n_H R^2 X^2	1.44e-8 −4.2992 0.9866 2.1008
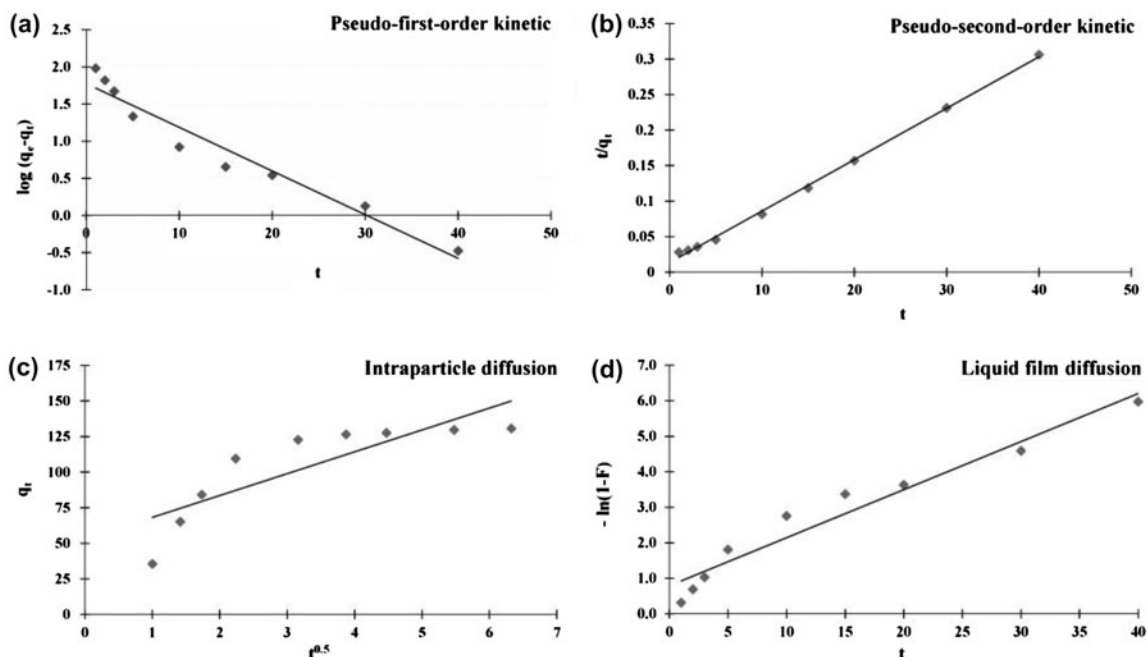
Fig. 5. Kinetic models for RB19 adsorption on f-MWCNTs: (a) Pseudo-first-order kinetic, (b) pseudo-second-order kinetic, (c) intraparticle diffusion, and (d) liquid film diffusion models.

Table 3
Kinetic models for the adsorption of RB19 onto f-MWCNTs

Kineticmodel	Equation	Definition of equation factors	Important parameters	Values
Pseudo-first-order	$\log(q_e - q_t) = \log q_e - \left(\frac{K_1 t}{2.303}\right)$ (7)	q_e = Adsorption capacity at equilibrium (mg g^{-1}) q_t = Adsorption capacity at time t (min) (mg g^{-1}) K_1 = The pseudo-first-order rate constant (min^{-1})	$q_{e,calc}$ $q_{e,exp}$ K_1 R^2	59.42 131.01 0.1354 0.9491
Pseudo-second-order	$\frac{t}{q_t} = \frac{1}{K_2 q_e^2} + \frac{t}{q_e}$ (8)	K_2 = The pseudo-second-order rate constant (g mg^{-1} s^{-1})	$q_{e,calc}$ $q_{e,exp}$ K_2 R^2	138.88 131.01 0.0038 0.9984
Intraparticle diffusion	$q_t = K_{int} t^{0.5} + C$ (9)	K_{int} = The intraparticle diffusion rate constant (mg g^{-1} min$^{-0.5}$) C = Indicator of boundary layer thickness	K_{int} C R^2	15.349 52.849 0.7029
Liquid film diffusion	$\ln(1 - F) = -K_{fd} t + C$ (10)	K_{fd} = The liquid film diffusion rate constant (min^{-1}) F = fractional attainment of equilibrium	K_{fd} C R^2	0.1353 0.7905 0.9491

adsorption capacities prevents this model to describe the adsorption rate.

3.9. Pseudo-second-order model

The pseudo-second-order kinetic model is based on the assumption that the rate-limiting step may be chemical adsorption involving valence forces through exchange or sharing of electrons between the adsorbate and adsorbent [50]. In this equation, adsorption capacity is assumed to be proportional to the number of active sites occupied on the adsorbent [39]. As it is implied from Fig. 5(b) and Table 3, this model fits the experimental data quite well. Therefore, based on this model, it can be concluded that the physisorption of RB19 by the functionalized surface of f-MWCNTs is the main reason controlling the adsorption rate.

3.10. Diffusion models

In the case of organic compounds like dyes, the adsorption onto an adsorbent involves the following consecutive steps: (1) bulk solution transport, (2) external diffusion in the liquid film surrounding the adsorbent particles (film diffusion), (3) internal diffusion in liquid-containing pores and/or along the pore walls (intraparticle diffusion), and (4) adsorption of adsorbate on active sites [44,49]. The slowest step limits the adsorption rate and according to the literature, usually it is not the first and the last steps [44]. Therefore, it is presumed that either external diffusion in liquid film

or intraparticle diffusion is the rate-limiting step. In this study, liquid film diffusion equation and intraparticle diffusion model are fitted to experimental data for better understanding of adsorption dynamics.

Intraparticle diffusion model is usually used to determine the rate-limiting step and the main assumption of this model is that the film diffusion step is negligible and intraparticle diffusion is the only rate-controlling step [51]. Intraparticle model assumes that solute uptake varies almost proportionally with $t^{0.5}$ rather than t [52]. The value of C is obtained from the intercept and gives an indication of the thickness of the boundary layer and when it is equal to zero, the sole rate-limiting step of the adsorption process is intraparticle diffusion [53]. According to Fig. 5(c) and Table 3, a large deviation from the origin and a high C value were obtained, which means that the intraparticle diffusion model is not the sole rate-limiting step of the adsorption process and there is a thick boundary layer around the f-MWCNTs when RB19 molecules are adsorbed.

In film diffusion step, the boundary layer plays the most significant role in adsorption during the transport of the solute molecules from the liquid phase to solid phase [52]. A linear plot of—ln (1 − F) vs. t that passes through origin would suggest that the liquid film diffusion is predominant in adsorption procedure [49]. As it is presented in Fig. 5(d) and Table 3, a very small aberration from the origin and higher R^2 value than the intraparticle diffusion model, indicates that the film diffusion is the most rate-controlling step in RB19 removal using f-MWCNTs.

Overall, it can be derived from Fig. 5 and Table 3, that the adsorption of RB19 using f-MWCNTs best fits to pseudo-second-order kinetic model and its diffusion state follows liquid film diffusion equation. Therefore, the adsorption's rate is predominantly controlled by a diffusion step mostly happening in external liquid film and the main reason for this rate-limiting phase is physisorption of RB19 molecules into the adsorption sites.

4. Conclusions

The main findings of this study are summarized as below:

(1) For maximum RB19 removal efficiency (95.15%) using f-MWCNTs, the optimum adsorption parameters are as follows: Agitation time = 20 min, adsorbent dose = 0.6 g L^{-1}, initial dye concentration = 50 mg L^{-1}, and pH 3.
(2) The adsorption process followed Langmuir and Temkin isotherms, which indicates that the monolayer and homogenous adsorption is predominant. Maximum adsorption capacity was found to be 217.39 mg g^{-1} that is relatively high, in comparison with adsorption capacities of the other anionic dyes onto MWCNTs.
(3) The adsorption kinetics followed pseudo-second-order model with a diffusion step almost fitting to liquid film diffusion equation. These results imply that the external diffusion in liquid film during physisorption of RB19 by f-MWCNTs is mainly the rate-limiting step of the adsorption process rather than intraparticle diffusion.

In light of the aforementioned conclusions, it can be expressed that functionalized MWCNTs prepared by the method explained in this study can be used as excellent adsorbents for removal of RB19 from aqueous solutions, while they possess a superb potential for removing the other anionic dyes.

Acknowledgments

References

[1] C. He, X. Hu, Functionalized ordered mesoporous carbon for the adsorption of reactive dyes, Adsorption 18 (2012) 337–348.

[2] M.I. El-Barghouthi, A.H. El-Sheikh, Y.S. Al-Degs, G.M. Walker, Adsorption behavior of anionic reactive dyes on H-type activated carbon: Competitive adsorption and desorption studies, Sep. Sci. Technol. 42 (2007) 2195–2220.

[3] E. Basturk, M. Karatas, Decolorization of antraquinone dye Reactive Blue 181 solution by UV/H$_2$O$_2$ process, J. Photochem. Photobiol., A Chem. 299 (2015) 67–72.

[4] E. Errais, J. Duplay, F. Darragi, I. M'Rabet, A. Aubert, F. Huber, G. Morvan, Efficient anionic dye adsorption on natural untreated clay: Kinetic study and thermodynamic parameters, Desalination 275 (2011) 74–81.

[5] U. Isah A., G. Abdulraheem, S. Bala, S. Muhammad, M. Abdullahi, Kinetics, equilibrium and thermodynamics studies of C.I. Reactive Blue 19 dye adsorption on coconut shell based activated carbon, Int. Biodeterior. Biodegrad. 102 (2015) 265–273.

[6] M. Taheri, M.R. Alavi Moghaddam, M. Arami, Techno-economical optimization of Reactive Blue 19 removal by combined electrocoagulation/coagulation process through MOPSO using RSM and ANFIS models, J. Environ. Manage. 128 (2013) 798–806.

[7] J.R. Guimarães, M.G. Maniero, R.N. de Araujo, A comparative study on the degradation of RB-19 dye in an aqueous medium by advanced oxidation processes, J. Environ. Manage. 110 (2012) 33–39.

[8] M.A.N. Khan, M. Siddique, F. Wahid, R. Khan, Removal of reactive blue 19 dye by sono, photo and sonophotocatalytic oxidation using visible light, Ultrason. Sonochem. 26 (2015) 370–377.

[9] F. Abu Bakar, J.Y. Ruzicka, I. Nuramdhani, B.E. Williamson, M. Holzenkaempfer, V.B. Golovko, Investigation of the photodegradation of Reactive Blue 19 on P-25 titanium dioxide: Effect of experimental parameters, Aust. J. Chem. 68 (2015) 471–480.

[10] J.E.B. McCallum, S.A. Madison, S. Alkan, R.L. Depinto, R.U. Rojas Wahl, Analytical studies on the oxidative degradation of the reactive textile dye uniblue A, Environ. Sci. Technol. 34 (2000) 5157–5164.

[11] X. Jiang, K. Cai, J. Zhang, Y. Shen, S. Wang, X. Tian, Synthesis of a novel water-soluble chitosan derivative for flocculated decolorization, J. Hazard. Mater. 185 (2011) 1482–1488.

[12] J.G. Qu, N.N. Li, B.J. Liu, J.X. He, Preparation of BiVO$_4$/bentonite catalysts and their photocatalytic properties under simulated solar irradiation, Mater. Sci. Semicond. Process. 16 (2013) 99–105.

[13] A. Pirkarami, M.E. Olya, S. Tabibian, Treatment of colored and real industrial effluents through electrocoagulation using solar energy, J. Environ. Sci. Health., Part A Environ. Sci. 48 (2013) 1243–1252.

[14] M. Siddique, R. Farooq, Z.M. Khan, Z. Khan, S.F. Shaukat, Enhanced decomposition of reactive blue 19 dye in ultrasound assisted electrochemical reactor, Ultrason. Sonochem. 18 (2011) 190–196.

[15] H. Wang, Q. Li, N. He, Y. Wang, D. Sun, W. Shao, K. Yang, Y. Lu, Removal of anthraquinone reactive dye from wastewater by batch hydrolytic-aerobic recycling process, Sep. Purif. Technol. 67 (2009) 180–186.

[16] G. McKay, M. Hadi, M.T. Samadi, A.R. Rahmani, M.S. Aminabad, F. Nazemi, Adsorption of reactive dye from aqueous solutions by compost, Desalin. Water Treat. 28 (2011) 164–173.

[17] J. Mittal, V. Thakur, A. Mittal, Batch removal of hazardous azo dye Bismark Brown R using waste material hen feather, Ecol. Eng. 60 (2013) 249–253.

[18] A. Mittal, Use of hen feathers as potential adsorbent for the removal of a hazardous dye, Brilliant Blue FCF, from wastewater, J. Hazard. Mater. 128 (2006) 233–239.

[19] A. Mittal, J. Mittal, in: S.K. Sharma (Ed.), Green Chemistry for Dyes Removal from Wastewater: Research Trends and Applications, Scrivener Publishing LLC, Beverly 2015, pp. 409–457.

[20] J. Mittal, D. Jhare, H. Vardhan, A. Mittal, Utilization of bottom ash as a low-cost sorbent for the removal and recovery of a toxic halogen containing dye eosin yellow, Desalin. Water Treat. 52 (2014) 4508–4519.

[21] G. Sharma, M. Naushad, D. Pathania, A. Mittal, G.E. El-desoky, Modification of *Hibiscus cannabinus* fiber by graft copolymerization: Application for dye removal, Desalin. Water Treat. 54 (2015) 3114–3121.

[22] C.H. Wu, Adsorption of reactive dye onto carbon nanotubes: Equilibrium, kinetics and thermodynamics, J. Hazard. Mater. 144 (2007) 93–100.

[23] H. Daraei, A. Mittal, M. Noorisepehr, J. Mittal, Separation of chromium from water samples using eggshell powder as a low-cost sorbent: Kinetic and thermodynamic studies, Desalin. Water Treat. 53 (2015) 214–220.

[24] A. Mittal, Adsorption kinetics of removal of a toxic dye, Malachite Green, from wastewater by using hen feathers, J. Hazard. Mater. 133 (2007) 196–202.

[25] H. Daraei, A. Mittal, J. Mittal, H. Kamali, Optimization of Cr(VI) removal onto biosorbent eggshell membrane: Experimental and theoretical approaches, Desalin. Water Treat. 52 (2014) 1307–1315.

[26] E. Radaei, M.R. Alavi Moghaddam, M. Arami, Removal of reactive blue 19 from aqueous solution by pomegranate residual-based activated carbon: Optimization by response surface methodology, J. Environ. Health Sci. Eng. 12 (2014) 65–73.

[27] A. Özcan, Ç. Ömeroğlu, Y. Erdoğan, A. Safa Özcan, Modification of bentonite with a cationic surfactant: An adsorption study of textile dye Reactive Blue 19, J. Hazard. Mater. 140 (2007) 173–179.

[28] X. Jiang, Y. Sun, L. Liu, S. Wang, X. Tian, Adsorption of C.I. Reactive Blue 19 from aqueous solutions by porous particles of the grafted chitosan, Chem. Eng. J. 235 (2014) 151–157.

[29] F. Çiçek, D. Özer, A. Özer, A. Özer, Low cost removal of reactive dyes using wheat bran, J. Hazard. Mater. 146 (2007) 408–416.

[30] M.H. Dehghani, A. Naghizadeh, A. Rashidi, E. Derakhshani, Adsorption of reactive blue 29 dye from aqueous solution by multiwall carbon nanotubes, Desalin. Water Treat. 51 (2013) 7655–7662.

[31] V.K. Gupta, R. Kumar, A. Nayak, T.A. Saleh, M.A. Barakat, Adsorptive removal of dyes from aqueous solution onto carbon nanotubes: A review, Adv. Colloid Interface Sci. 193–194 (2013) 24–34.

[32] J. Ghobadi, M. Arami, H. Bahrami, N. Mohammad Mahmoodi, Modification of carbon nanotubes with cationic surfactant and its application for removal of direct dyes, Desalin. Water Treat. 52 (2014) 4356–4368.

[33] H. Gao, S. Zhao, X. Cheng, X. Wang, L. Zheng, Removal of anionic azo dyes from aqueous solution using magnetic polymer multi-wall carbon nanotube nanocomposite as adsorbent, Chem. Eng. J. 223 (2013) 84–90.

[34] W. Konicki, I. Pełech, E. Mijowska, I. Jasińska, Adsorption of anionic dye Direct Red 23 onto magnetic multi-walled carbon nanotubes-Fe$_3$C nanocomposite: Kinetics, equilibrium and thermodynamics, Chem. Eng. J. 210 (2012) 87–95.

[35] A.K. Mishra, T. Arockiadoss, S. Ramaprabhu, Study of removal of azo dye by functionalized multi walled carbon nanotubes, Chem. Eng. J. 162 (2010) 1026–1034.

[36] F. Avilés, J.V. Cauich-Rodríguez, L. Moo-Tah, A. May-Pat, R. Vargas-Coronado, Evaluation of mild acid oxidation treatments for MWCNT functionalization, Carbon 47 (2009) 2970–2975.

[37] H. Sadegh, R. Shahryari-Ghoshekandi, S. Agarwal, I. Tyagi, M. Asif, V.K. Gupta, Microwave-assisted removal of malachite green by carboxylate functionalized multi-walled carbon nanotubes: Kinetics and equilibrium study, J. Mol. Liq. 206 (2015) 151–158.

[38] Y. Xing, L. Li, C.C. Chusuei, R.V. Hull, Sonochemical oxidation of multiwalled carbon nanotubes, Langmuir 21 (2005) 4185–4190.

[39] A. Azizi, M.R. Alavi Moghaddam, M. Arami, Removal of a reactive dye using ash of pulp and paper sludge, J. Residuals Sci. Technol. 9 (2012) 159–168.

[40] N.K. Amin, Removal of direct blue-106 dye from aqueous solution using new activated carbons developed from pomegranate peel: Adsorption equilibrium and kinetics, J. Hazard. Mater. 165 (2009) 52–62.

[41] A. Nejib, D. Joelle, A. Fadhila, G. Sophie, T.A. Malika, Adsorption of anionic dye on natural and organophilic clays: Effect of textile dyeing additives, Desalin. Water Treat. 54 (2015) 1754–1769.

[42] S. Karaca, A. Gürses, Ö. Açışlı, A. Hassani, M. Kıranşan, K. Yıkılmaz, Modeling of adsorption isotherms and kinetics of Remazol Red RB adsorption from aqueous solution by modified clay, Desalin. Water Treat. 51 (2013) 2726–2739.

[43] A. Khaled, A. El Nemr, A. El-Sikaily, O. Abdelwahab, Removal of Direct N Blue-106 from artificial textile dye effluent using activated carbon from orange peel: Adsorption isotherm and kinetic studies, J. Hazard. Mater. 165 (2009) 100–110.

[44] M.M.F. Silva, M.M. Oliveira, M.C. Avelino, M.G. Fonseca, R.K.S. Almeida, E.C. Silva Filho, Adsorption of an industrial anionic dye by modified-KSF-montmorillonite: Evaluation of the kinetic, thermodynamic and equilibrium data, Chem. Eng. J. 203 (2012) 259–268.

[45] J. Febrianto, A.N. Kosasih, J. Sunarso, Y.H. Ju, N. Indraswati, S. Ismadji, Equilibrium and kinetic studies in adsorption of heavy metals using biosorbent: A summary of recent studies, J. Hazard. Mater. 162 (2009) 616–645.

[46] R.R. Krishni, K.Y. Foo, B.H. Hameed, Adsorption of methylene blue onto papaya leaves: Comparison of linear and nonlinear isotherm analysis, Desalin. Water Treat. 52 (2014) 6712–6719.

[47] N. Mohammad Mahmoodi, A. Maghsoodi, Kinetics and isotherm of cationic dye removal from multicomponent system using the synthesized silica nanoparticle, Desalin. Water Treat. 54 (2015) 562–571.

[48] M. Hadi, M.R. Samarghandi, G. McKay, Equilibrium two-parameter isotherms of acid dyes sorption by

activated carbons: Study of residual errors, Chem. Eng. J. 160 (2010) 408–416.

[49] M. Ahmad, R.T. Bachmann, M.A. Khan, R.G.J. Edyvean, U. Farooq, M.M. Athar, Dye removal using carbonized biomass, isotherm and kinetic studies, Desalin. Water Treat. 53 (2015) 2289–2298.

[50] F. Ahmad, W.M.A. Wan Daud, M.A. Ahmad, R. Radzi, Cocoa (*Theobroma cacao*) shell-based activated carbon by CO_2 activation in removing of cationic dye from aqueous solution: Kinetics and equilibrium studies, Chem. Eng. Res. Des. 90 (2012) 1480–1490.

[51] A. Öztürk, E. Malkoc, Adsorptive potential of cationic Basic Yellow 2 (BY2) dye onto natural untreated clay (NUC) from aqueous phase: Mass transfer analysis, kinetic and equilibrium profile, Appl. Surf. Sci. 299 (2014) 105–115.

[52] S. Haider, F.F. Binagag, A. Haider, A. Mahmood, N. Shah, W.A. Al-Masry, S.U. Khan, S.M. Ramay, Adsorption kinetic and isotherm of methylene blue, safranin T and rhodamine B onto electrospun ethylenediamine-grafted-polyacrylonitrile nanofibers membrane, Desalin. Water Treat. 55 (2015) 1609–1619.

[53] Y. Kismir, A.Z. Aroguz, Adsorption characteristics of the hazardous dye Brilliant Green on Saklıkent mud, Chem. Eng. J. 172 (2011) 199–206.